

# Free Energy Calculations Reveal the Origin of Binding Preference for Aminoadamantane Blockers of Influenza A/M2TM Pore

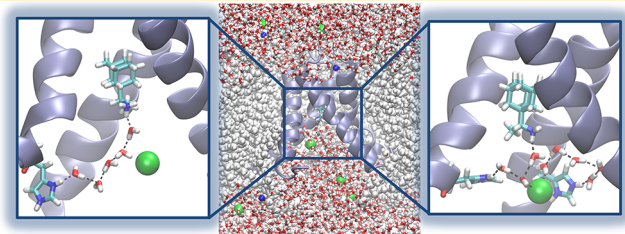
Paraskevi Gkeka,<sup>†</sup> Stelios Eleftheratos,<sup>‡</sup> Antonios Kolocouris,<sup>\*,‡</sup> and Zoe Cournia<sup>\*,†</sup>

<sup>†</sup>Biomedical Research Foundation of the Academy of Athens, 4 Soranou Ephessiou, 11527 Athens, Greece

<sup>‡</sup>Faculty of Pharmacy, Department of Pharmaceutical Chemistry, University of Athens, Panepistimioupolis-Zografou, 15771 Athens, Greece

## Supporting Information

**ABSTRACT:** Aminoadamantane derivatives, such as amantadine and rimantadine, have been reported to block the M2 membrane protein of influenza A virus (A/M2TM), but their use has been discontinued due to reported resistance in humans. Understanding the mechanism of action of amantadine derivatives could assist the development of novel potent inhibitors that overcome A/M2TM resistance. Here, we use Free Energy Perturbation calculations coupled with Molecular Dynamics simulations (FEP/MD) to rationalize the thermodynamic origin of binding preference of several aminoadamantane derivatives inside the A/M2TM pore. Our results demonstrate that apart from crucial protein–ligand intermolecular interactions, the flexibility of the protein, the water network around the ligand, and the desolvation free energy penalty to transfer the ligand from the aqueous environment to the transmembrane region are key elements for the binding preference of these compounds and thus for lead optimization. The high correlation of the FEP/MD results with available experimental data ( $R^2 = 0.85$ ) demonstrates that this methodology holds predictive value and can be used to guide the optimization of drug candidates binding to membrane proteins.

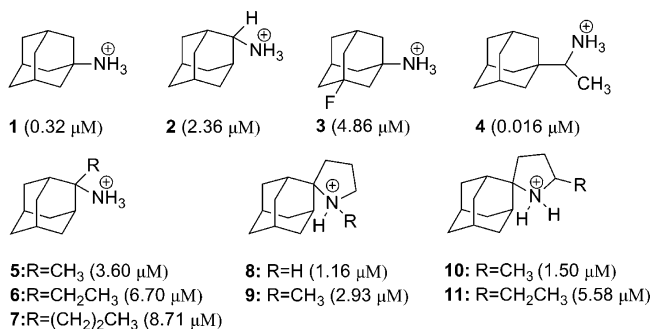


## 1. INTRODUCTION

Influenza A viruses can be occasionally transmitted from wild birds to humans and may give rise to devastating pandemics. In the effort to block influenza A virus, two main classes of anti-influenza agents have been discovered, neuraminidase and M2 protein inhibitors.<sup>1</sup> The M2 protein of influenza A virus is a tetrameric protein and its transmembrane domain (A/M2TM) comprises the pore of a proton channel that is activated by low pH in the viral endosome. Its activation ultimately leads to the unpacking of the influenza viral genome and to pathogenesis.<sup>2</sup> The main class of A/M2TM blockers is adamantane derivatives, such as amantadine **1** and rimantadine **4** (Scheme 1), which have been reported to block the M2 proton conducting channel. However, due to resistance of humans to amantadine and rimantadine, there is an urgent need to develop novel A/M2TM inhibitors.<sup>3–5</sup> Understanding the mechanism of action of amantadine derivatives could assist the development of novel potent inhibitors that overcome A/M2TM resistance.

The structure of the transmembrane region of A/M2TM, where aminoadamantane derivatives bind, has been recently unveiled.<sup>6–8</sup> A/M2TM is blocked by amantadine via a pore-blocking mechanism, which occludes the pore and blocks the proton conduction at low pH.<sup>6,9–13</sup> Moreover, ssNMR data demonstrated that the amantadine ammonium group is pointing toward the C-terminal.<sup>10</sup> In an effort to understand the mechanism of inhibition of the A/M2TM channel by aminoadamantanes, a series of computational studies has been performed over the last years. Molecular Dynamics (MD)

**Scheme 1. Structures of Compounds 1–11 Used in This Work and Respective Binding Constants to A/M2TM Protein Taken from Ref 44**



simulations indicated that aminoadamantanes inhibit A/M2TM channel activity by electrostatic hindrance due to their positively charged ammonium group.<sup>14</sup> In a different effort to explain the pore blocking mechanism and drug resistance, the water wiring theory was used in the wild type and S31N mutant of A/M2TM.<sup>15</sup> In another MD study, Wang et al. showed that the amantadine – M2TM complex remains stable during an 80-ns simulation; amantadine **1** is stabilized inside the M2TM pore through favorable interactions of the apolar adamantyl group

**Received:** October 16, 2012

with the Val27 “valve” and a hydrogen bond network formed between the ammonium group, water molecules, and carbonyl groups in the proximity of the C-terminal.<sup>16</sup> The nature of amantadine binding was also investigated by MD simulations for both high and low pH structures, showing that amantadine is stable inside the tetrameric bundle for 4 ns in both conditions.<sup>17</sup> Despite the extensive ongoing research on the A/M2TM inhibition mechanisms, currently no efficient methodology exists to explain the differences in binding preference for aminoadamantane derivatives, which is crucial for the design of novel potent drugs.

Ligand binding underlies a wide variety of recognition processes that often remain underdescribed due to insufficient resolution of experimental techniques. The use of reliable computational methods to calculate protein–ligand binding affinities can greatly enhance our understanding of such systems and can lead to the fast and efficient development of novel, potent protein inhibitors. The most commonly used methodologies in studies of protein–ligand binding affinities include, among others, docking, which usually ignores solvent contributions and/or protein flexibility, continuum electrostatic methods, such as the Molecular Mechanics/Poisson–Boltzmann Surface Area (MM/PBSA) and Molecular Mechanics/Generalized Born Surface Area (MM/GBSA) techniques, and Free Energy Perturbation (FEP) calculations. MM/PBSA and MM/GBSA techniques have been successfully used in various protein–ligand studies,<sup>18,19</sup> but their performance is system-dependent.<sup>20,21</sup> Also, it has been shown that these approaches are not accurate enough to direct lead optimization.<sup>22</sup> Recent work augmented the MM-GBSA methodology with information from explicit solvent simulations, which improved the binding affinity predictions relative to simple MM-GBSA.<sup>23,24</sup> Despite the above-mentioned improvements in the MM/PBSA and MM/GBSA methodologies, FEP calculations, given a sufficiently small  $\lambda$  and adequate sampling, are currently the most accurate qualitative link between experimental and computational studies.<sup>25–29</sup> However, to our knowledge, calculation of relative free energies of ligand binding in membrane proteins using the FEP methodology has been performed only for a limited number of systems and ligand alchemical transformations.<sup>30,31</sup> In this study, we use FEP/MD calculations to explore the thermodynamic origin of binding preference of eleven aminoadamantane derivatives inside the A/M2TM pore (Scheme 1). The results demonstrate that the flexibility of the system plays a crucial role in the interplay between ligand and membrane protein as it influences ligand location within the pore. Moreover, it is shown that the binding affinity of the ligands for the A/M2TM pore is a balance between hydrogen bonding ability, electrostatic and van der Waals interactions as well as the desolvation penalty for each ligand to leave the aqueous phase and enter the A/M2TM pore. The calculated binding free energy differences are in strong agreement with the experimental values indicating that this strategy can be applied in the lead optimization of A/M2TM blockers and provide insights for the origin of binding preference of close analogs.

## 2. METHODS

**2.1. Docking Calculations.** Four different protein structures were used for the docking calculations. In Systems 1 and 2, the protein structure of the A/M2TM-amantadine complex (residues 22–46 of the M2 protein) represents an equilibrated structure resulting from an MD simulation; the

source structure was taken from the final snapshot of a 17-ns MD simulation of the A/M2TM crystal structure (3C9J.pdb) in a fully hydrated membrane environment at acidic pH.<sup>17</sup> Docking was performed without water molecules (System 1) and including water molecules at a distance less than 9 Å from the position of amantadine (System 2). The final system (System 2) included nine water molecules in the A/M2TM pore. All four histidine residues (His37) were protonated for both System 1 and System 2. For the next two systems, the crystal structure of A/M2TM (PDB code: 3C9J.pdb)<sup>6</sup> with three (System 3) and four (System 4) protonated histidine residues (His37) was used. The “System Builder” module of Desmond software package was employed to solvate the system and water molecules at a distance of 9 Å from amantadine were kept.<sup>32–34</sup> Finally, eight water molecules were included in the pore for System 3 and System 4. The ligands under investigation are shown in Scheme 1. The protonated ligands were built with Maestro 8.5 and minimized with the default Macromodel 9.6 force field (MMFFs)<sup>35</sup> prior to docking using the conjugate gradient method and a distance-dependent dielectric constant of 4.0 until a convergence value of 0.0001 kJ/Å·mol was reached.

Glide 5.7 (Schrodinger, LLC) and GOLD 4.1 were used to carry out docking calculations of aminoadamantane derivatives (Scheme 1) in the four aforementioned systems.<sup>36–39</sup> Shortly, a thorough conformational search for a ligand is performed with Glide; then, all reasonable orientations (poses) for each low-energy conformer in the designated binding site are determined. In the process, the torsional degrees of the ligand are relaxed, whereas the protein conformation is fixed. A scoring function is then used to evaluate the ligand–protein binding affinity. The XP scoring function was used in the present study.<sup>39</sup> The “Protein Preparation” module of Glide was employed to add missing hydrogen atoms, assign protonation states, and run restrained minimization using the OPLS 2005 force field.<sup>40–42</sup> For the GOLD calculation, the ligands were docked into the A/M2TM binding site using the GoldScore function on System 2 and for atoms within 15 Å of amantadine 1.<sup>37</sup> The “allow early termination” command was deactivated. All the other parameters were set to GOLD default values, and the ligands were submitted to 100 genetic algorithm steps.

**2.2. Free Energy Perturbation Calculations.** Relative binding free energies were calculated using the Thermodynamic Cycle Perturbation method (TCP). In TCP, the relative change in binding free energy is calculated through nonphysical paths connecting a reference and a terminal state.<sup>25,43</sup> The relative solvation free energy difference,  $\Delta\Delta G_{\text{solv}}$ , between two ligands A and B can be calculated according to eq 1 based on Cycle 1 (Scheme 2)

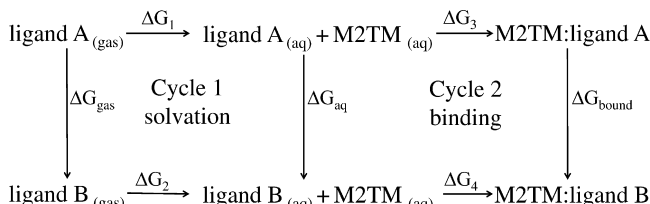
$$\Delta\Delta G_{\text{solv}} = \Delta G_2 - \Delta G_1 = \Delta G_{\text{aq}} - \Delta G_{\text{gas}} \quad (1)$$

where  $\Delta G_1$  and  $\Delta G_2$  are the free energies of transfer of A and B from the gas to the aqueous phase.  $\Delta G_{\text{gas}}$  and  $\Delta G_{\text{aq}}$  are the free energy differences of the mutation of A into B in vacuo and in aqueous solution, respectively. Moreover, Cycle 2 (Scheme 2) can be used to compute the difference in binding free energy between ligand A and ligand B given by

$$\Delta\Delta G_{\text{A} \rightarrow \text{B}} = \Delta G_4 - \Delta G_3 = \Delta G_{\text{bound}} - \Delta G_{\text{aq}} \quad (2)$$

where  $\Delta G_3$  and  $\Delta G_4$  are the free energies of transfer of A and B from the aqueous phase (unbound state) to the bound state.

**Scheme 2. Thermodynamic Cycle Used To Compute the Free Energy Differences<sup>a</sup>**



<sup>a</sup>ΔG<sub>1</sub>, ΔG<sub>2</sub>, ΔG<sub>3</sub>, and ΔG<sub>4</sub> are the free energies of transfer of A and B from the gas to the aqueous phase (unbound state) and from the aqueous phase to the bound state, respectively. ΔG<sub>gas</sub> and ΔG<sub>aq</sub> are the free energy differences of the mutation of A into B in vacuo and in aqueous solution, respectively, whereas ΔG<sub>bound</sub> is the free energy difference of the mutation of A into B bound to the protein.

ΔG<sub>bound</sub> is the free energy difference of the mutation of A into B with the ligands bound to protein.

FEP calculations combined with all-atom MD simulations were carried out using the Desmond MD package, version 2.4, as distributed by Schrodinger.<sup>33,34,36</sup> For the FEP/MD simulations in the bound state, two systems were considered: (i) a hydrated A/M2TM system with the protein backbone restrained and (ii) the A/M2TM protein (unrestrained) in a fully hydrated DPPC lipid bilayer. The crystallographic structure of the receptor–ligand complex (3C9J.pdb) was used to build the initial protein structure. The key histidine residues (His37) as well as the ligands were protonated. The ligands were built using the Maestro software with the initial pose of each ligand being the one obtained from the Glide docking calculations. Sodium and chloride ions were added at a concentration of 100 mM NaCl, to mimic the experiment used as reference in the present study.<sup>44</sup> Ions were randomly placed outside the A/M2TM pore. For the membrane–protein system, the ligand–receptor complex was embedded in a DPPC lipid bilayer and solvated with water using the “System Builder” utility available in Desmond.

The OPLS 2005 force field<sup>40–42</sup> was used to model all protein and ligand interactions, and the TIP3P model<sup>45</sup> was used for water. The particle-mesh Ewald method (PME)<sup>46</sup> was employed to calculate long-range electrostatic interactions with a grid spacing of 0.8 Å. van der Waals and short-range electrostatic interactions were smoothly truncated at 9.0 Å. The Nosé-Hoover thermostat<sup>47</sup> was utilized to maintain the constant simulation temperature, and the Martina-Tobias-Klein method<sup>47</sup> was used to control the pressure. The equations of motion were integrated using the multistep RESPA integrator<sup>48</sup> with an inner time step of 2.0 fs for bonded interactions and nonbonded interactions within the short-range cutoff. An outer time step of 6.0 fs was used for nonbonded interactions beyond the cutoff. Periodic boundary conditions were applied. For the vacuum simulations, minimization using the steepest descent method with a maximum of 2,000 steps was performed. Then, the system was relaxed using two NVT simulations at 10 and 325 K, respectively. Finally, a 2-ns NVT simulation at 325 K was used. For the FEP/MD calculations in unbound and bound state, a different protocol was used. In short, two rounds of steepest descent minimization were performed with a maximum of 2,000 steps and 10,000 steps and a harmonic restraint of 50 kcal/mol/Å<sup>2</sup> was applied on all solute atoms. Next, a series of four MD simulations was performed. The first simulation was performed at 10 K in the

NVT ensemble with the solute heavy atoms restrained with a force constant of 50 kcal/mol/Å<sup>2</sup>, followed by an identical simulation in the NPT ensemble. Subsequently, the temperature was raised to 325 K in the NPT ensemble and the force constant retained. Finally, a 2-ns equilibration was performed at 325 K in the NPT ensemble with all restraints removed (the protein backbone was restrained in the case of the membrane-free system). A temperature of 325 K was used in our MD simulations in order to be well above the melting temperature of DPPC lipids, which is 315 K. The above-mentioned equilibration was followed by a 2-ns NPT simulation for each window of the FEP calculation. In the case of ligands containing a cyclic group the equilibration and the sampling time were 3 ns each. Within this time, the total energy and RMSD of the systems reached a plateau, and the systems were considered equilibrated. The analysis of the trajectories was performed with the Gromacs and VMD tools<sup>49–51</sup> and in-house programs. For the calculation of hydrogen bonds, a cutoff angle of 30° between the donor-hydrogen-acceptor atoms and a cutoff distance of 3.5 Å between the donor and acceptor atoms were applied. The snapshots of the different poses were created with Maestro or VMD.<sup>36,51</sup>

The λ schedule used for calculating the relative free energy difference between two compounds A and B had 12 windows (Table S1, SI). The configurations of the system were saved in 4-ps intervals. In total, for each mutation, 96 ns (or 108 ns for the ligands containing a cyclic group) of sampling were performed summing to a total of approximately 2.2 μs of simulations for all the mutations.

**2.3. Stability of the Systems during the MD Simulations.** Convergence of all FEP calculations was checked by plotting the relative free energies ΔG over varying time ranges (an example is shown in Figure 1 and all the convergence plots for the membrane bound/unbound simulations can be found in the Supporting Information (SI), Figures S1–S18). The Bennett Acceptance Ratio (BAR) method was used to estimate the free energy difference from the MD simulations (for more details see the SI).<sup>52</sup> The errors in the relative free energies were calculated with the block bootstrapping method<sup>53</sup> using the default scheme applied in Desmond. Shortly, in block bootstrapping the data are divided into blocks of observations and is sampled randomly with replacement. Bootstrapping measures the computational uncertainty, which arises from the finite nature of the simulation, both in time and in space. A small bootstrap-estimated variance, as the ones calculated in our calculations, indicates a well equilibrated run, and thus sampling of our ensemble. Similarly small errors are common in FEP calculations.<sup>54,55</sup>

Analysis of the MD trajectories showed that the RMSD of the protein heavy atoms varies between 1.0 to 2.5 Å with the largest values occurring for the bulkier ligands like rimantadine (data not shown). As expected, the largest deviations are observed in the vicinity of Ala30, where the ligands bind. Moreover, secondary structure analysis of the M2TM protein shows that the α-helical motifs in the TM region are well conserved throughout the trajectory for all different MD simulations and compounds (an example is shown in Figure S19, SI).

The mutations considered in the present study refer to the ligands shown in Scheme 1. For two of the mutations, namely 1 to 2 and 1 to 4, intermediate stages (multistage FEP) were considered in order to sufficiently sample the configurational

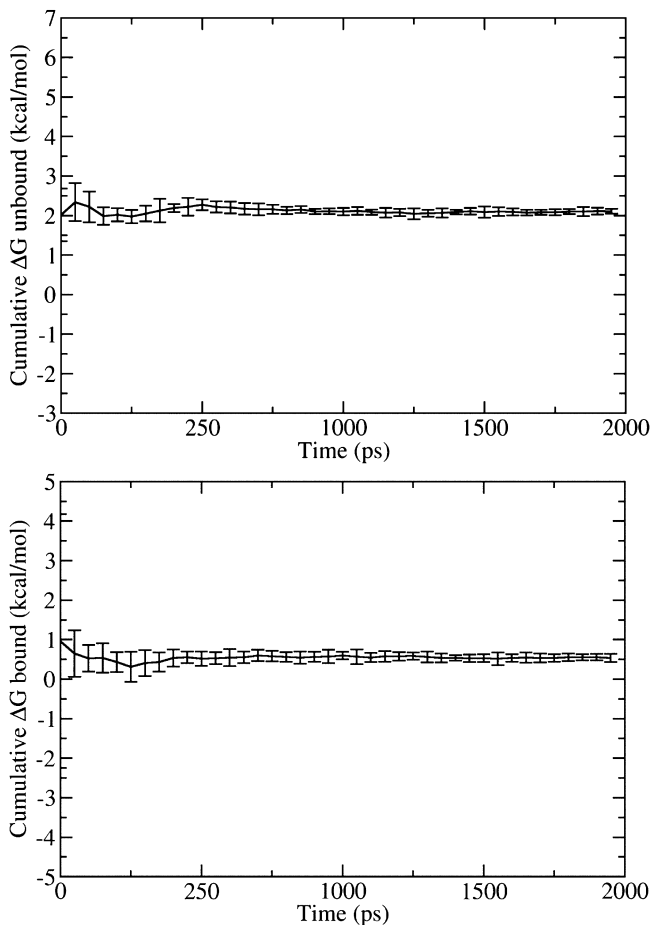
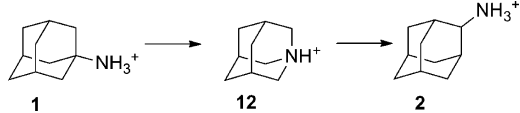


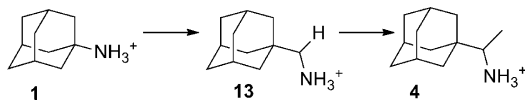
**Figure 1.** Cumulative free energy differences,  $\Delta G$ , over different time ranges for the 3 → 1 mutation, unbound (top) and bound (bottom) systems (flexible M2TM protein embedded in a DPPC lipid bilayer).

ensembles between the two ligands (Schemes 3 and 4).<sup>55</sup> These intermediate stages were chosen in order to ensure that

**Scheme 3. Multistage FEP Approach Applied for the Mutation from Ligand 1 to Ligand 2**



**Scheme 4. Multistage FEP Approach Applied for the Mutation from Ligand 1 to Ligand 4**



the total charge of the system is conserved while performing a FEP mutation. While it was previously shown that changing the total charge during a FEP calculation yielded results consistent with experimental data,<sup>56</sup> in our study this approach led to inconsistent results. More specifically, FEP calculations from 1 to 2 and from 1 to 4 starting from a positively charged molecule and using a neutral intermediate yielded a hysteresis between forward and backward mutations above 2 kcal/mol. Previous studies have shown that turning on or off a charge in a system

during a FEP calculation is nontrivial when using PME for the treatment of electrostatics.<sup>57,58</sup> The problem arises mainly from the fact that a charge change in PME is handled by introducing a uniform neutralizing background charge to enforce neutrality.<sup>59</sup> In FEP calculations this means that instead of calculating the free energy of turning off/on a charge, the calculated free energy is the sum of turning off/on the charge and the free energy of turning on/off a uniform neutralizing background charge, which might introduce an error in the overall difference in the free energy of binding.

### 3. RESULTS AND DISCUSSION

**3.1. Docking Calculations.** The results from the docking calculations for the different protein models and water scenarios (Systems 1–4) are presented in SI, Table S2. The correlation between docking and experimental binding affinities is minimal to low (Figure S20, SI), which indicates that docking calculations cannot reproduce the experimental data and thus a more accurate approach such as FEP/MD calculations should be adopted. The GoldScore function performs slightly better resulting in a correlation ( $R^2$ ) of 0.18. Despite this low correlation, Gold calculations predict that the ligand ammonium group is hydrogen bonded with neighboring water molecules, mediating a hydrogen bond network with the protonated His37 residue in accordance to available experimental data.<sup>10</sup>

**3.2. FEP/MD Calculations and the Effect of Protein Flexibility.** In an effort to reduce computational time, FEP calculations were initially performed in the absence of a membrane, using backbone constraints on the protein in aqueous solution in order to avoid unfolding. The correlation between the calculated relative binding free energies and the experimental binding affinities obtained by using this approach is low ( $R^2 = 0.20$ ) (Table 1 and Figure 2 (a)), as in the case of our docking results (Figure S20, SI). This low correlation can be attributed to the limited flexibility of the protein in the system, as the use of a “frozen” environment introduces a dependency of the free energies of binding on the selection of the protein structure, as discussed elsewhere.<sup>60</sup> To check this hypothesis, FEP/MD calculations were subsequently performed using a fully flexible system, with the A/M2TM protein embedded in a DPPC lipid bilayer. Interestingly, these calculations were in good agreement with the experimental binding affinities (Table 1, Figure 2 (b)), and the correlation with the experimental relative binding free energies was dramatically improved ( $R^2 = 0.85$ ).

To account for the failure of the rigid protein calculations to correlate with experimental results and in order to gain insights into the effect of protein flexibility on the binding of aminoadamantane derivatives, analysis of the protein structure and dynamics was performed. The A/M2TM pore diameter at residue Val27 was calculated for both systems with the restrained and the flexible protein backbone. It was found that by taking into account protein flexibility, the pore diameter increases by approximately 1 Å (from being 5 Å in the restrained system it becomes 6 Å in the flexible system). Due to lack of flexibility of the pore size, the ligands in the constrained system were systematically forced away from Val27 and toward the C-terminal of the pore, as indicated by the average distance of the ligands from the plane defined by the center of mass of the four Val27 residues (Table S3, SI). This longer distance between the ligands and Val27 is likely to alter not only the van der Waals interactions of the apolar adamantyl group with

**Table 1.** Summary of the FEP/MD Results and Comparison with the Experimental Data (in kcal/mol)

mutation	experiment		FEP/MD	
	$\Delta\Delta G_{\text{bind}}^a$	$\Delta\Delta G_{\text{bind}}^b$	$\Delta\Delta G_{\text{bind}}^c$	$\Delta\Delta G_{\text{solv}}$
(1)→(4)	-1.79	0.41 ± 0.66	-2.49 ± 0.61	2.83 ± 0.35
(1)→(2)	1.19	-8.47 ± 0.63	1.33 ± 0.41	0.73 ± 0.35
(1)→(3)	1.62	3.12 ± 0.49	1.57 ± 0.09	-1.55 ± 0.13
(5)→(6)	0.37	-1.92 ± 0.52	0.81 ± 0.17	1.43 ± 0.17
(6)→(7)	0.16	-1.28 ± 0.51	-0.19 ± 0.15	0.68 ± 0.15
(8)→(9)	0.55	-1.66 ± 0.66	0.25 ± 0.39	3.54 ± 0.33
(8)→(10)	0.15	N/A	0.34 ± 0.14	2.02 ± 0.14
(10)→(11)	0.78	-0.09 ± 0.50	0.31 ± 0.15	0.61 ± 0.15

<sup>a</sup>Experimental relative binding free energies were estimated according to  $\Delta\Delta G_{\text{exp}} = -k_B T \ln k_d^A/k_d^B = \Delta G_A - \Delta G_B$ . <sup>b</sup>Relative binding free energies for the system with the restrained protein in aqueous solution. <sup>c</sup>Relative binding free energies for the system with the flexible protein embedded in a membrane.

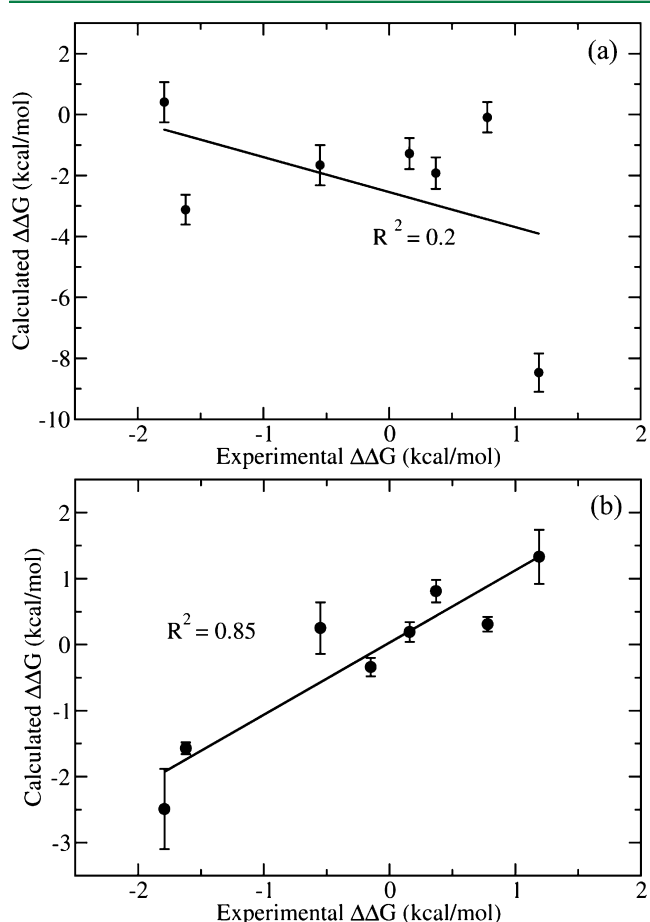


**Figure 2.** Correlation between experimental binding affinities and FEP calculated  $\Delta\Delta G$  for (a) the system with the restrained protein in aqueous solution and (b) the flexible protein in the DPPC lipid bilayer. The error bars were calculated using the block bootstrap method.

Val27 but also the hydrogen bond network between ligands, water molecules, and His37 leading to nonreliable  $\Delta\Delta G$  values (see values of calculated relative binding free energy for mutations 1→4, 5→6 in Table 1). For example, the hydrogen bonding ability of rimantadine 4 is underestimated in the system with the restrained protein (see Figure 3, ligand 4). Moreover, lack of protein flexibility does not allow discrimination between close analogs like 1 and 2 as indicated by the large deviation between the experimental and calculated values for the restrained system and the close agreement for the

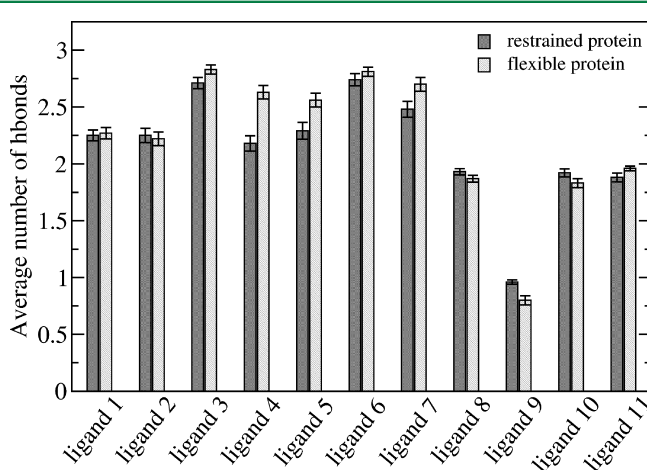


**Figure 3.** Average number of hydrogen bonds between the ammonium group of the different ligands and water molecules for the system with the restrained protein in aqueous solution and the system with the flexible protein embedded in a DPPC lipid bilayer. The error bars correspond to the standard error of the number of hydrogen bonds.

flexible system (Table 1). In particular, the pore diameter close to the ammonium group has a difference of approximately 1 Å in the flexible protein (from 8.2 Å for 1 it becomes 7.5 Å for 2). This difference cannot be captured in the system with the restrained protein, where the pore diameter does not change. In addition, the calculated bundle tilt with respect to the membrane normal for the different ligands in the flexible protein system varied between 32° and 38° relative to the membrane plane in agreement with previous studies,<sup>61,62</sup> while it was zero for the restrained system. This bundle tilt change reflects differences in tetramer flexibility; this plasticity is necessary for calculating correctly the different ligand binding affinities in A/M2TM. While this backbone flexibility is not needed for other nonmembrane receptor pocket clefts, where keeping the protein backbone rigid yields accurate results,<sup>55</sup> it seems crucial in the case of membrane proteins.

**3.3. Relative Solvation Free Energy Results.** The relative solvation free energy difference for the different ligands was also calculated (Table 1). Interestingly, the relatively high and positive value of  $\Delta\Delta G_{\text{solv}}$  for the amantadine 1 to rimantadine 4 mutation (2.83 kcal/mol) indicates that 1 has an increased desolvation free energy penalty compared to 4. This is of special relevance to the A/M2TM channel and generally to membrane proteins because, in contrast to water-soluble proteins, the ligand has to be transferred from the

extracellular aqueous environment to the binding site crevice in the transmembrane domain. Thus, ligands targeting membrane proteins must be, in most of the cases, almost entirely desolvated to bind to the receptor. For the **1** to **3** mutation, a negative relative solvation free energy ( $-1.55\text{ kcal/mol}$ ) was obtained indicating that the 3-fluoro-amantadine **3** has to overcome a higher desolvation free energy penalty compared to amantadine **1**. This value of  $\Delta\Delta G_{\text{solv}}^{1 \rightarrow 3}$  is in agreement with experimental results, as fluorine addition generally decreases lipophilicity of saturated aliphatic compounds, while it results in lipophilicity increase of aromatic rings.<sup>42,63,64</sup> Moreover, the experimentally measured binding affinities showed that **1** has a higher binding constant than **3**, which may be partly attributed to the higher desolvation penalty of **3** relative to **1** although compound **3** appears to have the highest number of hydrogen bonds (Figure 3).

Compounds **5–7** are 2-substituted-2-aminoadamantane derivatives, where the 2-substituent varies from Me (**5**) to Et (**6**) or n-Pr (**7**). In general, the positive  $\Delta\Delta G_{\text{solv}}$  values of the transformation of compound **5** to **6** ( $1.43\text{ kcal/mol}$ ) and **6** to **7** ( $0.68\text{ kcal/mol}$ ) indicate that by increasing the alkyl side chain size the desolvation free energy penalty is reduced. Similarly, compound **8** is less hydrophobic than compounds **9** and **10**, and thus it has to pay a higher desolvation penalty to be transferred from the solvent to vacuum as indicated by the relative solvation free energies (Table 1). Interestingly, the hydrogen to methyl change in the **8** to **9** and **10** to **11** mutations gives significantly different desolvation penalties ( $3.54$  and  $0.61\text{ kcal/mol}$ , respectively). Although in both cases (mutation of ligand **8** to **9** and **10** to **11**) a hydrogen atom is replaced by a methyl group, in the **8** to **9** mutation the change occurs on a protonated amine, while in **10** to **11** the hydrogen to methyl change occurs on an uncharged pyrrolidinium carbon. It has been experimentally shown that upon *N*-alkylation, protonated amines experience much higher solvation free energies than upon C-alkylation.<sup>64,65</sup> For example, the experimental  $\Delta\Delta G_{\text{solv}}$  of methylammonium to dimethylammonium is  $6.5\text{ kcal/mol}$ , while the  $\Delta\Delta G_{\text{solv}}$  of dimethylammonium with respect to *N*-methylpropan-1-ammonium is  $0.5\text{ kcal/mol}$ .<sup>64</sup> Our results show that *N*-methylation of the protonated amino group (**8** to **9** mutation) leads to a  $\Delta\Delta G_{\text{solv}} = 3.54\text{ kcal/mol}$  as compared to the C-methylation of an uncharged carbon of the pyrrolidinium ring (**10** to **11** mutation) with a  $\Delta\Delta G_{\text{solv}} = 0.61\text{ kcal/mol}$ , which lie well within the expected relative solvation free energies for protonated amines.

The  $\Delta\Delta G_{\text{solv}}$  values for the mutations **1** to **2**, **10** to **11**, **5** to **6**, and **6** to **7** are close to the accuracy of the FEP method, and they show the correct desolvation penalty tendency, which is consistent with the increase in lipophilicity arising from these mutations.

**3.4. Structural Basis for Inhibition.** Analysis of the MD trajectories showed that throughout the simulation all amino-adamantane derivatives remain stable in the binding site spanning the pore region between Val27 and His37 with their ammonium group pointing toward the His37 residues, in agreement with the experimental findings and previous simulations studies.<sup>9,17,66</sup> Water-mediated hydrogen bonds between the ammonium group of the different ligands and imidazole NH groups of His37 are apparent throughout the simulations for all the compounds. Although initially placed outside the pore, in all cases, two or three chloride ions move inside the A/M2TM channel, close to the protonated histidine

residues, and remain at a distance of  $3.3\text{--}7.0\text{ \AA}$  from the ammonium group of the ligands.

The relative free energy differences in the bound state (receptor embedded in the membrane) and unbound state (aqueous solution) can provide interesting information on the nature of the effects contributing to the binding affinity differences. It should, however, be noted here that only the calculated changes in the free energy of binding or solvation  $\Delta\Delta G_{\text{A} \rightarrow \text{B}}$  or  $\Delta\Delta G_{\text{solv}}$  should be used to interpret the results and not the constituent quantities in eq 1 and 2 (Scheme 2), i.e. the free energy of the mutation of A into B with the ligands bound to the protein, in the aqueous phase or in the gas phase  $\Delta G_{\text{bound}}$ ,  $\Delta G_{\text{aq}}$  and  $\Delta G_{\text{gas}}$ , respectively. The values of  $\Delta G_{\text{bound}}$ ,  $\Delta G_{\text{aq}}$  or  $\Delta G_{\text{gas}}$  which have been used in previous studies to interpret relative changes in binding affinity,<sup>31</sup> have no physical meaning and cannot be used to judge whether the mutation will have any stabilizing/destabilizing effect in water versus in the receptor; one has to calculate the difference in the free energies of binding and hydration,  $\Delta\Delta G_{\text{A} \rightarrow \text{B}}$  and  $\Delta\Delta G_{\text{solv}}$ , respectively, to estimate any effect (Scheme 2).

The addition of the  $\text{CHCH}_3$  bridge between the 1-adamantyl group and the ammonium group of amantadine **1**, resulting in rimantadine **4**, causes a 20-fold higher binding affinity (Scheme 1).<sup>44</sup> In an effort to understand the underlying mechanism of this improvement in the binding affinity, also captured with the FEP/MD calculations performed in the present study (Table 1), analysis of the MD trajectories was performed. Amantadine **1** and rimantadine **4** have similar positions inside the pore with adamantane embraced by Val27 and Ala30 side chains forming hydrophobic contacts. The average distance between the C2 carbons of **1** and the side chain carbons of Ala30 was measured to be  $3.75 \pm 0.13\text{ \AA}$ . Moreover, the relevant mean distance between the C4 carbons of **1** and the side chain carbons of Val27 was  $5.63 \pm 0.35\text{ \AA}$ . The mean angle between the 3-fold axis of amantadine **1** was measured as  $12.2 \pm 5.6^\circ$ , which is close to the ssNMR measurements (Table S4, SI).<sup>9,10</sup> For rimantadine **4**, the relevant mean distances from Ala30 and Val27 were  $3.76 \pm 0.15\text{ \AA}$  and  $5.54 \pm 0.45\text{ \AA}$ , respectively, while its tilt varied similarly to **1**. Moreover, the pore diameter close to Ile33 is the same for **1** and **4**. The absence of pore broadening allows the methyl group of  $\text{CHCH}_3$  bridge to interact with Ile33 through favorable van der Waals contacts. In Figure 4, representative snapshots from the FEP/MD simulations for compounds **1** (top) and **4** (bottom) are presented. Interactions between the hydrophobic core of both ligands with Val27 and Ala30 stabilize the adamantane group in this position. Rimantadine **4** also forms apolar contacts with its additional carbon  $\text{CHCH}_3$  bridge with residues closer to the C-terminal of the A/M2TM pore and the interchain area, like Ile33, which are missing in **1** (Figure 4, bottom).

Water-mediated hydrogen bonds between the ammonium group of the different ligands and imidazole NH groups of His37 are apparent throughout the simulations for all the compounds, stabilizing the orientation of the ammonium group toward the C-terminal, in agreement with experimental data.<sup>10</sup> In Figure 5, representative snapshots from the simulation of rimantadine **4** are presented showing the whole system (middle) and close-ups depicting the water-mediated hydrogen bond networks between the polar ammonium group of rimantadine, chloride, and His37. To investigate the possible differences in the polar contacts between the ammonium group of the ligands and the neighboring water molecules, hydrogen bond analysis was performed (Figure 3). The results show that

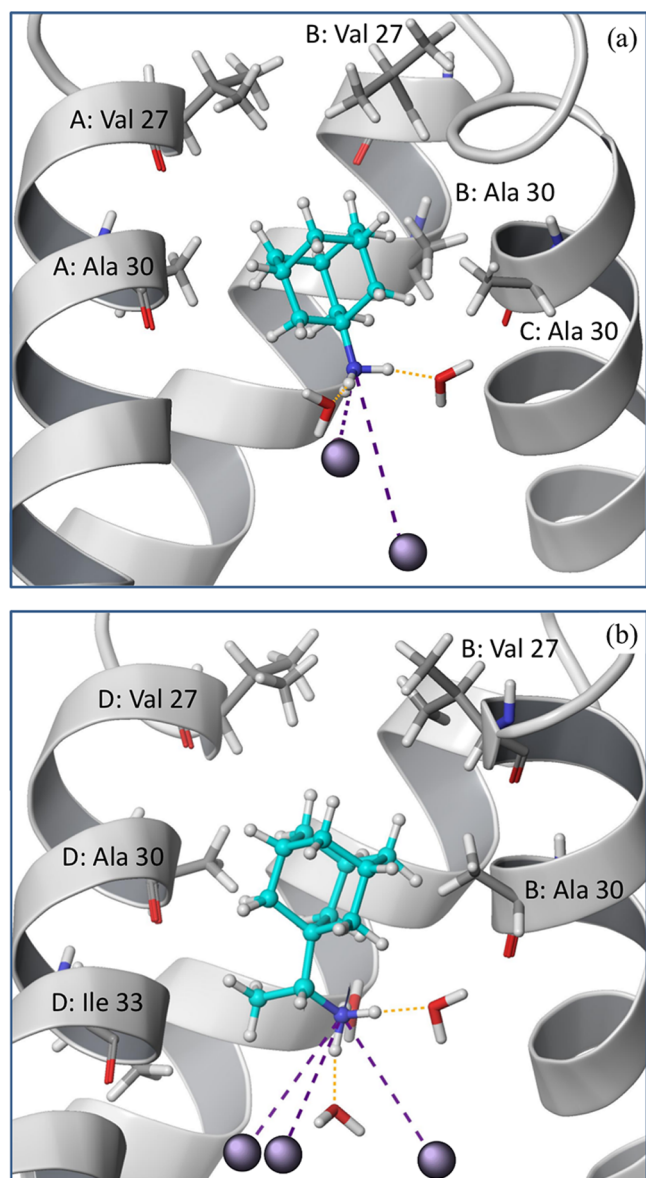


**Figure 4.** Representative snapshots from the FEP/MD simulations for (a) amantadine **1** and (b) rimantadine **4** A/M2TM blockers. Hydrogen bonds between the ammonium group and the neighboring water molecules as well as salt bridges with the chloride ions are shown with orange and purple dashed lines, respectively. Key hydrophobic residues Val27, Ala30, and Ile 33 are also shown in licorice representation.

amantadine forms on average two hydrogen bonds with neighboring water molecules, while rimantadine forms three hydrogen bonds with water molecules almost throughout the simulation time (Figure 3 and Figure 4). The increased hydrogen bonding ability of **4**, the additional hydrophobic interactions as well as the higher desolvation free energy compared to **1** may well explain the higher binding affinity of rimantadine to the A/M2TM channel. Moreover, salt bridges are formed between the positively charged ammonium group and the negatively charged chloride ions for both **1** and **4** (Figure 4). In the case of rimantadine **4** three chloride ions are within 6 Å and interact electrostatically with the ammonium group, while for amantadine **1** only two ions are present within the same distance from the ammonium group.

The ammonium-water radial distribution functions (RDFs),  $g(r)$ , for **1** and **4** in the unbound and bound states, in both the restrained and flexible protein systems, were also calculated (Figure S21, SI). The first and second solvation shell occupancies were estimated from the respective  $g(r)$  functions by integrating up to the first and second minima, respectively. The distributions in all three cases for both compounds exhibit a sharp peak at 2.8 Å, corresponding to the first hydration shell around the ammonium group. The associated first hydration shell coordination numbers as well as the coordination numbers for the second hydration shell are shown in Table 2. The RDFs for the amantadine **1** and rimantadine **4** in water and in the system with the restrained protein do not present any significant differences (Figure S21 (a) and (b), SI, Table 2). Nevertheless, in the fully flexible system, it is apparent that the first hydration shell at 2.8 Å is more distinct in the case of **4** compared to **1** resulting to first hydration shell coordination numbers of 2.8 and 3.3 for **1** and **4**, respectively. This can be attributed to the larger accessibility of the key ammonium group of rimantadine **4** (ammonium group connected to adamantane through the CHCH<sub>3</sub> bridge) to water molecules in the M2TM flexible channel compared with amantadine **1** (ammonium group connected directly to the bulky adamantyl moiety), which also leads to a better hydrogen bonding capability of **4** relative to **1** (Figure 3).

The calculated free energy of binding for 3-fluoro-1-adamantanamine **3** relative to amantadine **1** is 1.57 kcal/mol, in excellent agreement with the experimental result of 1.62 kcal/mol. Visual inspection of the trajectory of compound **3** did not reveal any bad van der Waals contacts between fluorine and the protein. Both ligands are positioned at the same location inside the pore, form the same intermolecular interactions with neighboring hydrophobic residues, and a similar number of hydrogen bonds with water, and have the same tilt with respect to the membrane normal. Although the two compounds form a similar number of hydrogen bonds, the lower affinity of **3** compared to **1** can be partly attributed to the formation of hydrogen bonds of reduced strength due to the lower  $pK_a$  of the ammonium group in 3-fluoro-amantadine compared to that of amantadine.<sup>63</sup> Moreover, based on our calculations, the difference in the binding affinities of the two compounds can be attributed to the higher desolvation penalty of **3** compared to **1** (Table 1). For compounds **5**, **6**, and **7**, the adamantyl moiety is turning around the C2–C6 axis (Figures S22, S23, SI) in order for the symmetric A/M2TM pore to accommodate the increasing alkyl group; the average angle between the pore axis and C–N bond vector increases progressively from 14.5° for **2**, 22.5° for **5**, to 38.6° for **6**, and to 50.4° for **7** (Figure S22, Table S4, SI); a subtle balance between hydrogen bonding and van der Waals interactions with A/M2TM key residues, like Val27 and Ala30, influences the ligand tilt inside the pore. It is also notable that the mobility of compounds **6** and **7** is limited compared to the mobility of compound **5** as indicated by the standard deviation of the tilt of the C–N bond relative to the pore axis (Table S4, SI). On transforming **5** through **7**, both the desolvation penalty and the binding affinity are reduced (Table 1). Visual inspection of the trajectories revealed bad van der Waals contacts between the adamantyl group of **7** with Ala30 and Ser31 and its propyl side chain with Ile33 (“Bad and Ugly contacts” module in Maestro, default contact cutoff ratios). Interestingly, these repulsive contacts were absent in the case of **5** due to the smaller alkyl chain and the change in the orientation, as apparent from the C–N bond vector (22.5° for

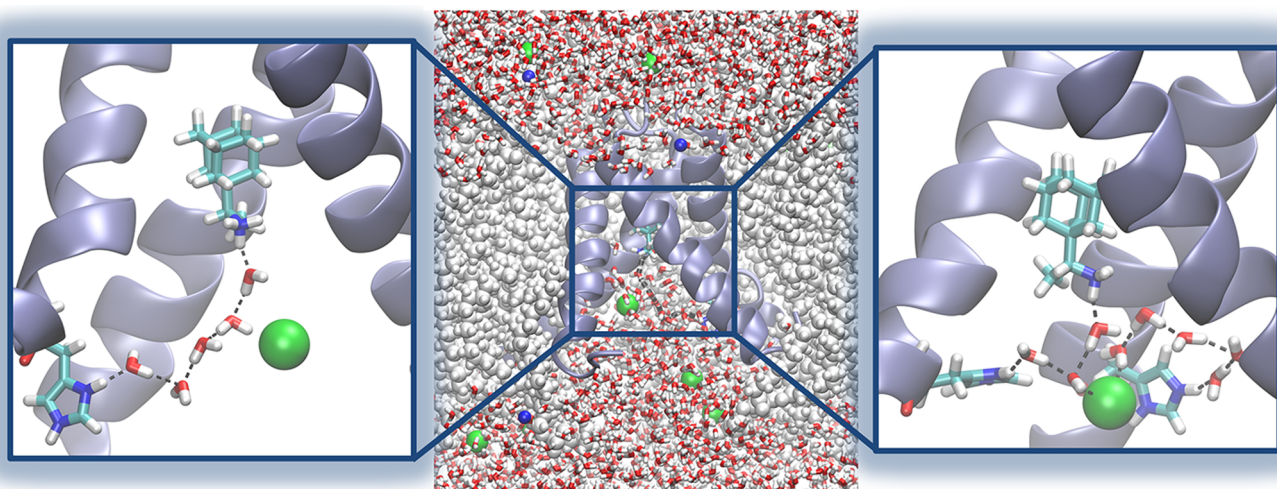


**Figure 5.** Representative snapshots from the simulation of rimantadine **4** bound to A/M2TM. In the left close-up of the pore, the hydrogen bond network between the ammonium group and His37 is depicted. In the right close-up, a hydrogen bond network that bridges the ammonium nitrogen, water, chloride, and His37 is shown.

**Table 2. First and Second Average Solvation Shells for Amantadine and Rimantadine in the Different Systems under Study**

	unbound		bound restrained protein		bound flexible protein	
	first shell	second shell	first shell	second shell	first shell	second shell
amantadine	3.7	27.4	2.7	9.4	2.8	5.3
rimantadine	3.7	26.9	2.7	10.6	3.3	6.0

**5** and 50.4° for **7**, Table S4, SI), which forces the adamantyl group toward the protein side chains in **7**. Moreover, the smaller alkyl chain of **5** allows the formation of a salt bridge between the ammonium group with a chloride ion, which is not observed in the case of **7**, as the n-propyl chain moves toward the C-terminal and shields the ammonium group from chloride ions. The above-mentioned observations support the reduced binding affinity of **7** compared to **5**. Unfortunately, in the current Desmond FEP/MD implementation it is not possible to quantify ligand-residue interaction energies throughout the trajectory, which would provide quantitative information for the above-mentioned interactions.

Considering the pyrrolidine derivatives **8–11**, the calculated values for the changes from **8** to **9** (0.25 kcal/mol), **8** to **10** (0.34 kcal/mol), and **10** to **11** (0.31 kcal/mol) are close to the experimental values (0.55, 0.15, and 0.78 kcal/mol, respectively). For the mutations **8** through **11** although the desolvation cost is reduced, the binding affinity is slightly decreased because of the increasing size of the ligand that has to be accommodated in the A/M2TM pore. This becomes obvious through comparison of compounds **8** to **10** and **11**, where the 5-substitution of the pyrrolidine ring increases in size from hydrogen to methyl and ethyl respectively, whereas at the same time hydrogen bonding ability remains similar for **8**, **10**, and **11** (Figure 3). Comparison of the *N*-methyl derivative **9** with its isomeric 5-methyl pyrrolidine **10** indicates that the lower activity of the former can be attributed to its substantial lower H-bonding ability. The bulky cyclic compounds **8–11** fall in the same subgroup with 2-alkyl-2-aminoadamantane derivatives **2**, **5–7**. Compounds **8**, **9**, and **10** have better binding affinity than 2-alkyl derivatives and even better or

similar to 2-amantadine **2**. Similarly to compound **7**, compounds **8**, **9**, and **10** are more lipophilic than **5** or **2**, and thus have similar or lower desolvation penalty. The higher affinity of compounds **8–10** compared to **7**, **5**, or **2** can be also attributed to better van der Waals interactions inside the pore as their hydrogen bonding ability is significantly lower (see Figure 3).

#### 4. CONCLUSIONS

Docking and FEP/MD calculations for different amino-adamantane derivatives were performed in order to establish a methodology that can successfully reproduce available experimental binding affinity data and provide insights into the molecular features by which different ligands bind the influenza A/M2TM pore. Docking calculations as well as FEP/MD calculations with a restrained A/M2TM protein system resulted in poor or low correlation with experimental data. An improved protocol, where protein flexibility of the system was taken into account by embedding the protein inside a fully hydrated lipid bilayer, was then considered. FEP/MD calculations were performed, yielding very good correlation with the available experimental data and indicating that protein flexibility dramatically improves the accuracy of FEP calculations for this system. Comparison between the different MD trajectories indicates that protein flexibility greatly influences ligand location inside the pore. A rigid protein system fixes the pore diameter around Val27, leading the compounds closer to the C-terminal compared to the systems with the flexible protein, and influences their hydrogen bonding ability.

For all ligands under investigation, the ammonium group points toward His37 and connects to it through water-mediated hydrogen bonds. The adamantyl moiety is placed in a hydrophilic pocket embraced by Val27 to Ala30 side chain groups. The polar group of the ligands is the key factor for their orientation, while the hydrophobic adamantyl moiety plays an important role regarding the positioning of each ligand along the A/M2TM pore. Chloride ions, although initially placed randomly outside the A/M2TM pore, enter the pore and remain close to His37 residues, at a distance of approximately 3.3–7.0 Å from the ammonium group of the ligands in all cases

and formed salt bridges with several of the aminoadamantanes derivatives.

The significance of ligand desolvation is described for the aminoadamantane ligands studied herein, suggesting for the first time an explanation for the higher affinity of rimantadine **4** relative to amantadine **1**. The binding interactions of the ligands inside the A/M2TM channel is a compromise between hydrogen bonding ability, which is elevated by a primary ammonium group, and van der Waals enthalpic and entropic contributions, which are increased by the ability of the lipophilic adamantyl moiety to adequately fill the hydrophobic pocket within the A/M2TM pore. Furthermore, the FEP calculations of the relative solvation free energy demonstrate that the desolvation penalties are a major contributor to the A/M2TM binding affinity and should be considered for drug design purposes targeting membrane-associated systems. The decrease in the penalty of ligand desolvation facilitates its entrance into the binding site crevice and thus higher binding affinity can be obtained. An additional carbon chain can reduce the desolvation cost and can result in the higher binding affinity of rimantadine **4** relative to amantadine **1**, but it can also diminish the favorable van der Waals intermolecular interactions inside the pore and reduce the binding affinity, as was observed for 2-alkyl-2-adamantanamines **5–7**. An additional carbon moiety is favorable when added between the adamantane carbon and ammonium group and not on the 2-adamantane ring position. Moreover, the addition of a cyclic carbon motif, as in compound **8**, is preferable to the linear branching in compounds **5–7**. Another example for the significance of desolvation cost to the binding affinity is provided by the addition of a fluorine group to the adamantyl group of amantadine **1**; the resulting compound, 3-fluoro-amantadine, has higher desolvation cost resulting to a reduced binding affinity. Moreover, although we gain 3.54 kcal/mol on desolvation free energy when mutating **8** to **9**, the addition of one methyl group on the ammonium group leads to the loss of one hydrogen bond donor group (N–H) for compound **9** (Figure 3). Thus, a delicate balance of hydrophobic contributions and intermolecular interactions is required for achieving enhanced ligand-protein binding in membrane protein systems.

In conclusion, we have established a protocol that utilizes FEP/MD calculations of relative binding free energies and desolvation free energy penalty to leave the aqueous phase in order to bind to the A/M2TM pore. This protocol comprises a successful methodology for structure-based drug design targeting ion channel pores. With the increasing computer power, it is envisaged that this methodology could be scaled up to design novel A/M2TM inhibitor scaffolds.

## ASSOCIATED CONTENT

### Supporting Information

FEP convergence graphs and further data analysis plots. This material is available free of charge via the Internet at <http://pubs.acs.org>.

## AUTHOR INFORMATION

### Corresponding Author

\*Phone: +30-210-7274834 (office), +30-210-7274315 (lab).  
Fax: +30-210-7274747. E-mail: [ankol@pharm.uoa.gr](mailto:ankol@pharm.uoa.gr) (A.K.).  
Phone: +30-210-6597195 (office), +30-210-6507568 (lab).  
Fax: +30-210-6597545. E-mail: [zcournia@bioacademy.gr](mailto:zcournia@bioacademy.gr) (Z.C.).

## Notes

The authors declare no competing financial interest.

## ACKNOWLEDGMENTS

The authors would like to thank Dr. Ekta Khurana for providing A/M2TM structures from MD simulations, Dr. James Watney for the insightful and stimulating discussions, and Dr. George Patargias and Harris Ioannidis for critically reading the manuscript. A.K. would like to thank Chiesi Hellas for a kind donation to support the work of S.E.

## REFERENCES

- (1) Lagoja, I. M.; De Clercq, E. *Med. Res. Rev.* **2008**, *28* (1), 1–38.
- (2) Helenius, A. *Cell* **1992**, *69* (4), 577–578.
- (3) Zhou, J.; Zou, L.; Zhang, X.; Liao, J.; Ni, H.; Hou, N.; Wang, Y.; Li, H.; Wu, J.; Jonges, M.; Meijer, A.; Koopmans, M.; Ke, C. *J. Clin. Microbiol.* **2011**, *49* (7), 2651–2655.
- (4) Sheu, T. G.; Fry, A. M.; Garten, R. J.; Deyde, V. M.; Shwe, T.; Bullion, L.; Peebles, P. J.; Li, Y.; Klimov, A. I.; Gubareva, L. V. *J. Infect. Dis.* **2011**, *203* (1), 13–17.
- (5) Bright, R. A.; Medina, M. J.; Xu, X. Y.; Perez-Oronoz, G.; Wallis, T. R.; Davis, X. H. M.; Povinelli, L.; Cox, N. J.; Klimov, A. I. *Lancet* **2005**, *366* (9492), 1175–1181.
- (6) Stouffer, A. L.; Acharya, R.; Salom, D.; Levine, A. S.; Di Costanzo, L.; Soto, C. S.; Tereshko, V.; Nanda, V.; Stayrook, S.; DeGrado, W. *Nature* **2008**, *451* (7178), 596–599.
- (7) Schnell, J. R.; Chou, J. J. *Nature* **2008**, *451* (7178), 591–595.
- (8) Acharya, R.; Carnevale, V.; Fiorin, G.; Levine, B. G.; Polishchuk, A. L.; Balannik, V.; Samish, I.; Lamb, R. A.; Pinto, L. H.; DeGrado, W. F.; Klein, M. L. *Proc. Natl. Acad. Sci. U. S. A.* **2010**, *107* (34), 15075–15080.
- (9) Cady, S. D.; Schmidt-Rohr, K.; Wang, J.; Soto, C. S.; Degrado, W. F.; Hong, M. *Nature* **2010**, *463* (7281), 689–692.
- (10) Cady, S. D.; Wang, J.; Wu, Y.; Degrado, W. F.; Hong, M. *J. Am. Chem. Soc.* **2011**, *133* (12), 4274–4284.
- (11) Chuang, G.-Y.; Kozakov, D.; Brenke, R.; Beglov, D.; Guarneri, F.; Vajda, S. *Biophys. J.* **2009**, *97* (10), 2846–2853.
- (12) Rosenberg, M. R.; Casarotto, M. G. *Proc. Natl. Acad. Sci. U. S. A.* **2010**, *107* (31), 13866–13871.
- (13) Gu, R.-X.; Liu, L. A.; Wei, D.-Q.; Du, J.-G.; Liu, L.; Liu, H. *J. Am. Chem. Soc.* **2011**, *133* (28), 10817–10825.
- (14) Leonov, H.; Astrahan, P.; Krugliak, M.; Arkin, I. T. *J. Am. Chem. Soc.* **2011**, *133* (25), 9903–9911.
- (15) Qin, G.; Yu, K.; Shi, T.; Luo, C.; Li, G.; Zhu, W.; Jiang, H. *J. Phys. Chem. B* **2010**, *114* (25), 8487–8493.
- (16) Wang, J.; Ma, C.; Fiorin, G.; Carnevale, V.; Wang, T.; Hu, F.; Lamb, A. R.; Pinto, H. L.; Hong, M.; Klein, L. M.; DeGrado, F. W. *J. Am. Chem. Soc.* **2011**, *133* (32), 12834–12841.
- (17) Khurana, E.; Devane, R. H.; Dal Peraro, M.; Klein, M. L. *Biochim. Biophys. Acta* **2011**, *1808* (2), 530–537.
- (18) Kuhn, B.; Kollman, P. A. *J. Med. Chem.* **2000**, *43* (20), 3786–3791.
- (19) Stoica, I.; Sadiq, S. K.; Coveney, P. V. *J. Am. Chem. Soc.* **2008**, *130* (8), 2639–2648.
- (20) Pearlman, D. A. *J. Med. Chem.* **2005**, *48* (24), 7796–7807.
- (21) Kuhn, B.; Gerber, P.; Schulz-Gasch, T.; Stahl, M. *J. Med. Chem.* **2005**, *48* (12), 4040–4048.
- (22) Jorgensen, W. L. *Acc. Chem. Res.* **2009**, *42* (6), 724–733.
- (23) Ravindranathan, K.; Tirado-Rives, J.; Jorgensen, W. L.; Guimaraes, C. R. W. *J. Chem. Theory Comput.* **2011**, *7* (12), 3859–3865.
- (24) Abel, R.; Salam, N. K.; Shelley, J.; Farid, R.; Friesner, R. A.; Sherman, W. *ChemMedChem* **2011**, *6*, 1049–1066.
- (25) Zwanzig, R. *J. J. Chem. Phys.* **1954**, *22* (8), 1420–1426.
- (26) Reddy, M. R.; Erion, M. D.; Agarwal, A. Free Energy Calculations: Use and Limitations in Predicting Ligand Binding Affinities. In *Reviews in Computational Chemistry*, 1st ed.; Lipkowitz, K.

- B., Boyd, D. B., Eds.; John Wiley & Sons, Inc.: Hoboken, NJ, USA, 2007; Vol. 16, pp 217–304.
- (27) Reddy, M. R.; Erion, M. D. *J. Am. Chem. Soc.* **2001**, *123* (26), 6246–6252.
- (28) Erion, M. D.; Dang, Q.; Reddy, M. R.; Kasibhatla, S. R.; Huang, J.; Lipscomb, W. N.; van Poelje, P. D. *J. Am. Chem. Soc.* **2007**, *129* (50), 15480–15490.
- (29) Lamb, M. L.; Jorgensen, W. L. *Curr. Opin. Chem. Biol.* **1997**, *1* (4), 449–457.
- (30) Zhao, C.; Caplan, D. A.; Noskov, S. Y. *J. Chem. Theory Comput.* **2010**, *6* (6), 1900–1914.
- (31) Gonzalez, A.; Murcia, M.; Benhamu, B.; Campillo, M.; Lopez-Rodriguez, M. L.; Pardo, L. *MedChemComm* **2011**, *2* (3), 160–164.
- (32) Bowers, K. J.; Chow, E.; Xu, H.; Dror, R. O.; Eastwood, M. P.; Gregersen, B. A.; Klepeis, J. L.; Kolossvary, I.; Moraes, M. A.; Sacerdoti, F. D.; Salmon, J. K.; Shan, Y.; Shaw, D. E. calable algorithms for molecular dynamics simulations on commodity clusters. In *Proceedings of the 2006 ACM/IEEE Conference on Supercomputing (SC06)*, Tampa, Florida, 2006.
- (33) *Desmond Molecular Dynamics System*, version 2.4; D. E. Shaw Research: New York, NY, 2010.
- (34) *Maestro-Desmond Interoperability Tools*, version 2.4; Schrodinger: New York, NY, 2010.
- (35) Halgren, T. A. *J. Comput. Chem.* **1996**, *17* (5–6), 616–641 and references therein.
- (36) *Maestro*, version 9.1; Schrodinger, Inc.: New York, NY, 2010.
- (37) Jones, G.; Willett, P.; Glen, R. C.; Leach, A. R.; Taylor, R. *J. Mol. Biol.* **1997**, *267* (3), 727–748.
- (38) Halgren, T. A.; Murphy, R. B.; Friesner, R. A.; Beard, H. S.; Frye, L. L.; Pollard, W. T.; Banks, J. L. *J. Med. Chem.* **2004**, *47* (7), 1750–1759.
- (39) Friesner, R. A.; Murphy, R. B.; Repasky, M. P.; Frye, L. L.; Greenwood, J. R.; Halgren, T. A.; Sanschagrin, P. C.; Mainz, D. T. J. *Med. Chem.* **2006**, *49* (21), 6177–6196.
- (40) Jorgensen, W. L.; Maxwell, D. S.; Tirado-Rives, J. *J. Am. Chem. Soc.* **1996**, *118* (45), 11225–11236.
- (41) Kaminski, G. A.; Friesner, R. A.; Tirado-Rives, J.; Jorgensen, W. L. *J. Phys. Chem. B* **2001**, *105* (28), 6474–6487.
- (42) Shivakumar, D.; Williams, J.; Wu, Y.; Damm, W.; Shelley, J.; Sherman, W. *J. Chem. Theory Comput.* **2010**, *6* (5), 1509–1519.
- (43) *Free energy calculations in rational drug design*; Reddy, M. R., Erion, M. D., Eds.; Kluwer Academic Publishers: New York, 2001.
- (44) Eleftheratos, S.; Ortore, G.; Kocolouris, A.; Martinelli, A.; Spearpoint, P.; Martin, S.; Hay, A. *Bioorg. Med. Chem. Lett.* **2010**, *20* (14), 4182–4187.
- (45) Jorgensen, W. L.; Chandrasekhar, J.; Madura, J. D.; Impey, R. W.; Klein, M. L. *J. Chem. Phys.* **1983**, *79* (2), 926–935.
- (46) Essmann, U.; Perera, L.; Berkowitz, M. L.; Darden, T.; Lee, H.; Pedersen, L. G. *J. Chem. Phys.* **1995**, *103* (19), 8577–8593.
- (47) Martyna, G. J.; Tobias, D. J.; Klein, M. L. *J. Chem. Phys.* **1994**, *101* (S), 4177–4189.
- (48) Humphreys, D. D.; Friesner, R. A.; Berne, B. J. *J. Phys. Chem.* **1994**, *98* (27), 6885–6892.
- (49) Berendsen, H. J. C.; van der Spoel, D.; van Drunen, R. *Comput. Phys. Commun.* **1995**, *91* (1–3), 43–56.
- (50) Hess, B.; Kutzner, C.; van der Spoel, D.; Lindahl, E. *J. Chem. Theory Comput.* **2008**, *4* (3), 435–447.
- (51) Humphrey, W.; Dalke, A.; Schulten, K. *J. Mol. Graphics* **1996**, *14* (1), 33–38.
- (52) Bennett, C. H. *J. Comput. Phys.* **1976**, *22* (2), 245–268.
- (53) Boyce, S. E.; Mobley, D. L.; Rocklin, G. J.; Graves, A. P.; Dill, K. A.; Shoichet, B. K. *J. Mol. Biol.* **2009**, *394*, 747–763.
- (54) Zeevaart, J. G.; Wang, L.; Thakur, V. V.; Leung, C. S.; Tirado-Rives, J.; Bailey, C. M.; Domaoal, R. A.; Anderson, K. S.; Jorgensen, W. L. *J. Am. Chem. Soc.* **2008**, *130* (29), 9492–9499.
- (55) Baggett, A. W.; Cournia, Z.; Han, M. S.; Patargias, G.; Glass, A. C.; Liu, S. Y.; Nolen, B. *J. ChemMedChem.* **2012**, *7* (7), 1286–1294.
- (56) Zhou, R.; Das, P.; Royyuru, A. K. *J. Phys. Chem. B* **2008**, *112* (49), 15813–15820.
- (57) Kastenholz, M. A.; Hunenberger, P. H. *J. Chem. Phys.* **2006**, *124* (12), 124106–124127.
- (58) Kastenholz, M. A.; Hunenberger, P. H. *J. Chem. Phys.* **2006**, *124* (22), 224501–224520.
- (59) Hummer, G.; Pratt, L. R.; Garcia, A. E. *J. Phys. Chem.* **1996**, *100* (4), 1206–1215.
- (60) Michel, J.; Foloppe, N.; Essex, J. W. *Mol. Inf.* **2010**, *29* (8–9), 570–578.
- (61) Cady, S. D.; Hong, M. *Proc. Natl. Acad. Sci. U.S.A.* **2008**, *105* (5), 1483–1488.
- (62) Wang, J.; Kim, S.; Kovacs, F.; Cross, T. A. *Protein Sci.* **2001**, *10* (11), 2241–2248.
- (63) Jasys, V. J.; Lombardo, F.; Appleton, T. A.; Bordner, J.; Ziliox, M.; Volkmann, R. A. *J. Am. Chem. Soc.* **2000**, *122* (3), 466–473.
- (64) Zhang, W.; Hou, T.; Qiao, X.; Xu, X. *J. Phys. Chem. B* **2003**, *107* (34), 9071–9078.
- (65) Sitkoff, D.; Sharp, K. A.; Honig, B. *J. Phys. Chem.* **1994**, *98* (7), 1978–1988.
- (66) Yi, M.; Cross, T. A.; Zhou, H. X. *J. Phys. Chem. B* **2008**, *112* (27), 7977–7979.